Electrical properties of filled silicone rubber

2000 J. Phys.: Condens. Matter 12 1873

(http://iopscience.iop.org/0953-8984/12/8/330)

J. Phys.: Condens. Matter **12** (2000) 1873–1897. Printed in the UK PII: S0953-8984(00)05786-6

Electrical properties of filled silicone rubber

Enis Tuncer and Stanislaw M Gubanski

High Voltage Division, Department of Electric Power Engineering, Chalmers University of Technology, 412 96 Gothenburg, Sweden

E-mail: enis.tuncer@elkraft.chalmers.se

Received 7 July 1999, in final form 16 December 1999

Abstract. Rubber materials for high-voltage outdoor applications have been studied. They were prepared as mixtures of silicone polymer with different concentrations of powdered aluminium trihydrate as a filler. The dielectric properties, $\chi^*(\omega) = \chi' - \mathrm{i}\chi''$, were measured at different temperatures using a low-frequency dielectric spectroscopy technique. Without any filler a classical interfacial relaxation was pronounced with dominating direct-current (dc) conduction in the losses, χ''. On increasing the concentration of filler, a low-frequency dispersion mechanism started to dominate the relaxation behaviour. On adding the filler, the dc conduction first decreased and then increased again after a certain concentration level was passed. This behaviour showed that the filler particles acted like scattering centres or traps for conduction when the concentration was low. As the concentration increased, the conductivity of the filler particles and of the interface (between the filler particles and the polymer matrix) started to dominate the conduction. Master curve shifts of the data showed an Arrhenius type of activation. The data were modelled by superposition of three different processes, Havriliak–Negami dipolar relaxation, dc conduction and low-frequency dispersion (hopping conduction) contributions, using a nonlinear least-squares fitting method.

1. Introduction

In order to tailor better composite materials for special purposes in electrical applications it is important to know which properties of their constituents, i.e. conductivity, dielectric permittivity, filler concentration, spatial distribution, shape of filler particles etc, are critical to the overall electrical properties of the composite. The electrical properties of composite systems have been studied extensively due to their applications in microelectronics and microwave technologies [1]. In the literature, most of the data refer to systems composed of two media [2, 3] and they mention little about frequency responses of the systems. Although experimental techniques for observing electrical properties of composites are accurate today, to understand and model the behaviour of these properties is not that easy [4].

Heterogeneous systems composed of two or more phases show different conductive and dielectric properties, depending on the properties of phases. The most studied cases among these have been binary mixtures in which the concentration of the more conductive medium was low [5–15]. In such cases, obviously, the spatial distribution of filler particles did not play an important role in the electrical properties of the system. A higher concentration of filler and its distribution throughout the matrix will change the local electric field and, therefore, the electrical properties [16].

The concentration of filler material influences polarization, as well as dc conduction and hopping conduction inside the material. Therefore, an increase in filler concentration will decrease the distance between filler particles and, depending on the frequency of the applied

0953-8984/00/081873+25$30.00

field, charges will be able to hop or tunnel between the filler particle islands [17]. Additionally, at a critical concentration value, the filler particles form paths that connect one end of the material to the other end (percolating clusters). On the other hand, dipolar relaxations are also present in the material. An addition of filler in the host medium creates the conditions for Maxwell–Wagner–Sillars polarization, due to the difference between the intrinsic electrical properties of the media [5]. Again, just like in hopping conduction, dipolar polarization will depend on the frequency of the applied field. There are other effects that also contribute to the electrical properties—i.e. space-charge relaxation and electrode effects—but these are excluded from this study. All the contributions to the electrical properties of the composite material were measured by the dielectric spectroscopy technique.

Conductive particle-filled polymer systems have been intensively studied [18, 19] due to their technological applications, for example as semiconducting layers and electromagnetic shields. In those studies, the concentration of the conductive phase (usually carbon black particles) has usually been around the percolation threshold [20, 21], in which case the filler particles form a chain like structure and connect two opposite sides of the composite. Another composite system, which has been investigated due to the well defined inclusion shapes, is glass-bead-filled polymer [22, 23]. Again, the concentration of the filler has exceeded the percolation threshold. Although the latter system has potential for application as electrical insulation, it does not have enough mechanical strength. In high-voltage engineering, on the other hand, different composite materials are used. One example is the application of filled elastomers, like silicone and ethylene-propylene-diene-monomer (EPDM) rubbers, in high-voltage outdoor insulation. In this study, in contrast to those of previously mentioned systems, a highly filled polymer system composed of polydimethylsiloxane (PDMS) polymer and α-aluminium trihydrate (ATH) was considered and its electrical properties were investigated using the dielectric spectroscopy technique in the frequency domain [24, 25]. Experimental data from dielectric spectroscopy were modelled by a combination of several processes, Havriliak–Negami dipolar relaxation, dc conduction and low-frequency dispersion (hopping conduction).

2. Theoretical background

The classical Debye dispersion relation with a single relaxation time, τ, is described as a function of angular frequency, ω, as

$$\varepsilon^*(\omega) = \varepsilon_{hf} + \frac{\varepsilon_s - \varepsilon_{hf}}{1 + \mathrm{i}\omega\tau} \tag{1}$$

where i and ε^* are $\sqrt{-1}$ and the complex dielectric permittivity of the material, respectively. The term $\varepsilon_s - \varepsilon_{hf}$ is called the relaxation strength, $\Delta\varepsilon$, where ε_s is the static dielectric permittivity and ε_{hf} is the dielectric permittivity at optical or high frequencies. A better parameter to use is the dielectric susceptibility, χ, instead of the dielectric permittivity; $\chi^* = \varepsilon^* - \varepsilon_{hf}$ and $\chi_s = \varepsilon_s - \varepsilon_{hf}$. χ_s is the dielectric susceptibility at $\omega = 0$ Hz.

From the experimental point of view, the dielectric responses of materials, except dilute solutions and ferroelectrics, do not show Debye response characteristics. For this reason, they are usually modelled by a modified Debye response (distribution of relaxation times):

$$\chi^*(\omega) = \frac{\chi_s}{[1 + (\mathrm{i}\omega\tau)^\alpha]^\beta}. \tag{2}$$

Here, α and β are parameters depending on the shape of the response. When $\alpha = \beta = 1$, we have the classical Debye process. The other famous responses with distributed relaxation times can be obtained when $\alpha = 1$ and $\beta \neq 1$, which gives the Cole–Davidson response, and

when $\alpha \neq 1$ and $\beta = 1$, which gives the Cole–Cole response. The general case, however, is the Havriliak–Negami dipolar relaxation ($\alpha \neq 1$ and $\beta \neq 1$).

One can, furthermore, separate the real and imaginary parts of dielectric susceptibility,

$$\chi^*(\omega) = \chi' - \mathrm{i}\chi''. \tag{3}$$

Here, the imaginary part is the loss associated with the dipoles in the material and the real part is the polarizability of the dipoles, proportional to the energy stored in the medium.

For example, if the dc conduction, σ_{dc}, is taken into account, its contribution can be observed only in the imaginary part of $\chi^*(\omega)$:

$$\chi^*(\omega) = \frac{\chi_s}{[1 + (\mathrm{i}\omega\tau)^\alpha]^\beta} + \frac{\sigma_{dc}}{\mathrm{i}\varepsilon_0\omega}. \tag{4}$$

There will be no contribution to χ' from the dc conduction.

As shown above, it is possible to distinguish the two independent processes, dipolar relaxation and dc conduction. However, as mentioned before, the presence of defects and disorder in the material will lead to a frequency-dependent complex conductivity which we will call hopping conductivity, σ_{ho}, which is also known as a low-frequency dispersion [4]:

$$\sigma_{ho}(\omega) = \frac{\varsigma}{\varepsilon_0(\mathrm{i}\omega)^\gamma} \tag{5}$$

where ς and γ are constant parameters, $0 < \gamma \leqslant 1$. When $\gamma = 1$, the equation reduces to the dc conduction term. This behaviour of conductivity (equation (5)) together with the contribution from dc conductivity is called power-law behaviour [4]. Hopping charge systems were first studied by Pollak and Geballe [26] and Mott and Davis [27]. Localized charge carriers in these systems may contribute to dielectric relaxation. The charge carriers, first, act like dipoles jumping between two potential wells (harmonic oscillation). Second, they move in the direction of the external electric field and contribute to the ac conduction. As can be observed from the above equation, the hopping conduction contribution to the dielectric response increases as the frequency of the applied electric field decreases. One can also get a similar kind of power-law behaviour when the relaxation times of the dipolar relaxations are distributed exponentially ($\sim \exp(\tau/\tau')$); however, it is a physical approach. Moreover, relaxations slower than ones observable in the experimental window used can also appear as power-law-like.

As a result, the complex dielectric susceptibility of a material can be explained in a general form as a function of angular frequency [28], ω, as follows:

$$\chi^*(\omega) = \frac{\chi_s}{(1 + (\mathrm{i}\omega\tau)^\alpha)^\beta} + \frac{\sigma_{dc}}{\mathrm{i}\varepsilon_0\omega} + \frac{\varsigma}{\varepsilon_0(\mathrm{i}\omega)^\gamma}. \tag{6}$$

Although the above equation explains the frequency response, dielectric susceptibility is also a function of temperature. The response usually does not change very drastically with temperature as long as the material does not alter its structure. The response preserves its shape; thus, this behaviour of the temperature dependence can be used to shift the data to obtain a single master curve [29]. Accordingly, the response at T_1 can be obtained by shifting the frequency of the response at T_2 by a factor A:

$$\chi^*(\omega; T_2) = \chi^*(A\omega; T_1). \tag{7}$$

This process implies a strong temperature dependence of the frequency of the dielectric susceptibility, and helps us to analyse polarization processes—not only for a wider range of frequencies, but also to find the activation energy for the process. It also improves the reliability of the data, since there will be additional data points in the graphs. The

temperature dependence of the shifts can be expressed as Arrhenius behaviour with an activation energy, W:

$$A(T) = \exp\left(-\frac{W}{kT}\right) \tag{8}$$

where A is the master curve shift factor of the dielectric susceptibility at a given temperature, T; k is the Boltzmann constant, 8.61×10^{-5} eV K^{-1}.

3. Experimental procedure

3.1. Materials

The basic silicone rubber material investigated was the commercially available formulation PowerSil™ 401/70S from Wacker Chemie AG, Germany, composed of PDMS and 20 wt% of powdered fumed silica. Surface-treated ATH powder was added to the elastomer as a filler. Table 1 shows the filler content of each sample in parts per hundred rubber (phr) and in wt%. The samples were prepared to observe the effect of the high concentration of the filler material on dielectric properties.

Table 1. Material labels and their ATH concentrations—in parts per hundred (phr) and in weight percentages.

Sample No	phr	wt%
1	0	0
2	25	20
3	50	33
4	100	50
5	150	60
6	200	67
7	250	71

To prepare the samples, ATH and elastomer were mixed in a blender at 12 rpm for 10 min at room temperature. Plates with a thickness of 1 mm and a diameter of 200 mm were compression moulded between Mylar™ sheets for 10 min at 135 °C and at 50 MPa. They were cured at 150 °C for 5 h. Afterwards, the samples were cut into smaller discs with a diameter of 120 mm for dielectric measurements. They were kept in a desiccator at atmospheric pressure and dry air to avoid any sorption of water into the material [22, 30, 31].

3.2. Dielectric spectroscopy measurements

In the dielectric spectroscopy technique, a sinusoidal voltage is applied across the sample and the current response is measured while the frequency of the applied voltage varies during the measurements. The ratio of the applied voltage to the measured current gives the complex impedance of the sample as a function of frequency. Therefore, one can obtain information about the complex dielectric susceptibility, $\chi^*(\omega)$, of the sample as a function of frequency in this way.

The dielectric responses of samples were measured using guarded brass electrodes having a diameter of 80 mm at seven temperatures, i.e. 30, 60, 90, 120, 90, 60 and 30 °C, between frequencies of 1 mHz and 1 kHz. The measurements were divided into two parts 'up' and 'down', which represent the temperature scheme's increasing and decreasing regions. In the first part (up) of the experiments, when starting to measure the dielectric response of a sample

at 30 °C, the temperature was increased in intervals of 30 °C up to 120 °C. Likewise, in the second part (down) of the experiments, using the last measurement of the first part at 120 °C as the starting measurement of the second part, the temperature was decreased in intervals of 30 °C down to 30 °C. Using an experimental procedure like this, one is able to check the stability of the samples and the reliability of dielectric data. In the text we have used 'up' and 'down', respectively, to represent the results obtained from these measurements.

3.3. Data analysis

A characteristic example of the family of real and imaginary parts of the dielectric permittivity ($\varepsilon^*(f)$) obtained from the experiments is presented in figure 1. In the figure, responses are

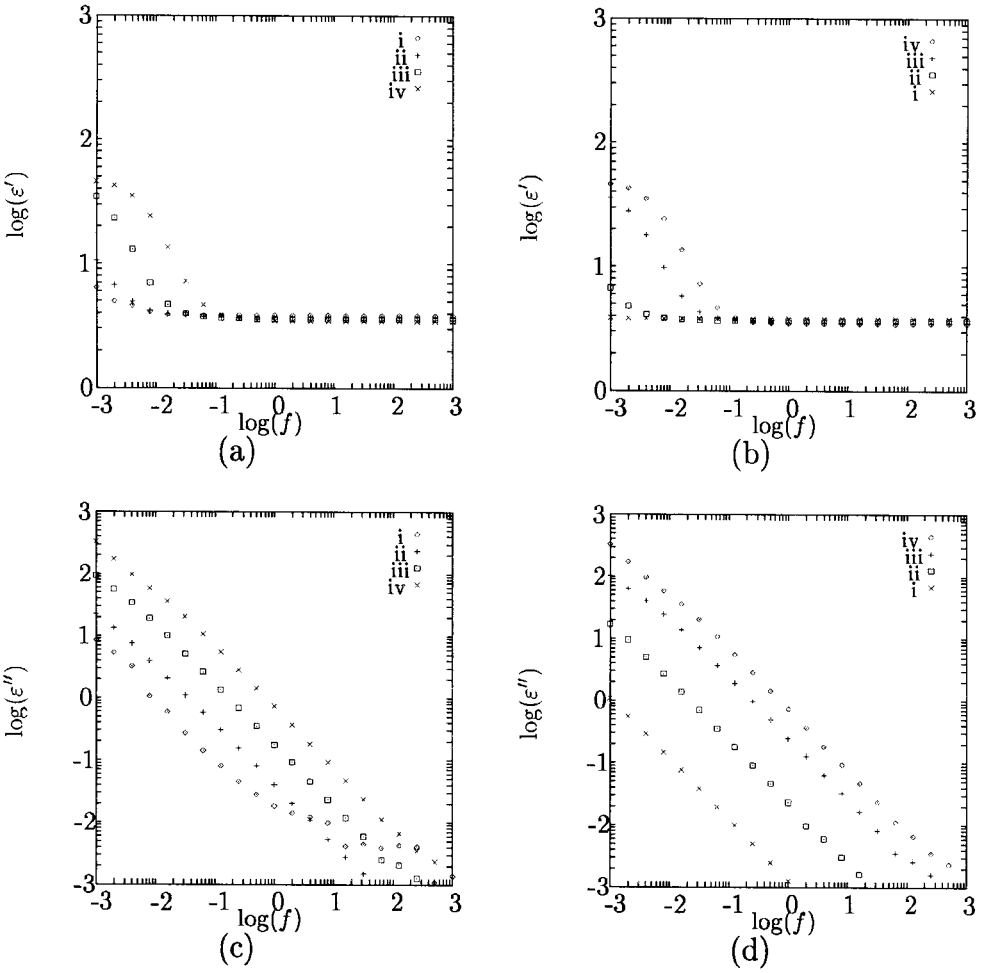

Figure 1. Real ((a), (b)) and imaginary ((c), (d)) parts of the dielectric permittivity of sample 1 (the concentration of the filler is 0 phr) at different temperatures as functions of frequency, $f = \omega/2\pi$, before the master curve shifts. Graphs (a) and (c) show the up temperature measurements and graphs (b) and (d) show the down temperature measurements. The labels (i), (ii), (iii) and (iv) represent 30, 60, 90 and 120 °C, respectively, which are the temperature values at which the measurements were carried out.

shown depending on the temperatures going up or down during the measurements. The real and imaginary parts of the dielectric permittivity are also separated in the figure. In the first stage of the data analysis, an average value of the real part of dielectric permittivity values at high frequencies, $\langle\varepsilon'\rangle$, of each response at different temperatures, was subtracted from the real parts of the responses, $\varepsilon'(f)$, to get the real parts of the susceptibilities, $\chi'(f)$. This was done by taking the ε'-values starting with the highest frequency, and moving towards the lowest, until ε' starts to increase. This ε'-value and the others towards the higher-frequency end were taken in the averaging:

$$\chi'(f) = \varepsilon(f) - \langle\varepsilon\rangle$$
$$\langle\varepsilon\rangle = \left[\sum_{i}^{n} \varepsilon_i'\right] \Big/ n \tag{9}$$

where n varies from 1 to the number of dielectric permittivity values that do not start to increase. Furthermore, this average dielectric permittivity value, $\langle\varepsilon\rangle$, was assigned as the dielectric permittivity at higher frequencies, ε_{hf}. The susceptibilities at different temperatures obtained from this procedure are presented in figure 2. There was one negative effect of the subtraction: the weak low-frequency dispersions might also be included in ε_{hf}.

Although ε_{hf} should be the same for each measurement, it spread over a narrow range of values. This occurred as a result of measurement inaccuracy. To increase the accuracy of the data for high frequencies, a compensation value for ε_{hf} was entered before the measurements were made. However, the measurements were automated and the initial compensation value was not changed for other measurements at different temperatures.

The dielectric response curves of samples that were regularly distributed over the frequency scale at different temperatures were horizontally shifted using equation (8) to obtain one master curve. Therefore, we have prepared two master curve responses as functions of the angular frequency, $\omega = 2\pi f$, for each sample for the up and down measurements.

4. Results

4.1. The system with 0% of ATH

For samples containing 0% of ATH, the dielectric permittivities at higher frequencies for the sample were 3.64 and 3.61 for up and down measurements, respectively. Assuming that there were no other dipolar relaxations at lower frequencies, the dielectric constant at $\omega = 0$ Hz, ε_s, for the sample becomes about 43. If we, first, examine the real part of $\chi^*(f)$ (figure 2), the shapes of the curves obtained in the up (figure 2(a)) and down (figure 2(b)) measurements change. The curve at the highest temperature (120 °C) shows a relaxation phenomenon where the low-frequency end of the response approaches a constant value in both measurements. The curves at higher temperatures shifted very regularly to lower frequencies on the angular frequency scale of the measurements. The spectra at low frequency and at low temperatures became more visible at higher temperatures when the frequency shifted. Second, the shape of the imaginary part of the susceptibility, $\chi''(f)$ (figures 2(c), 2(d)), was unaltered in both temperature regimes, but its position on the frequency scale again shifted very regularly to higher frequencies. By purely horizontal shifts of the curves, starting from the highest temperature towards the lowest one, good temperature–frequency superpositions (master curves) of all responses were obtained, both for the temperatures going up and those going down in the measurements. The master curves are shown in figure 3 at a reference temperature of 30 °C.

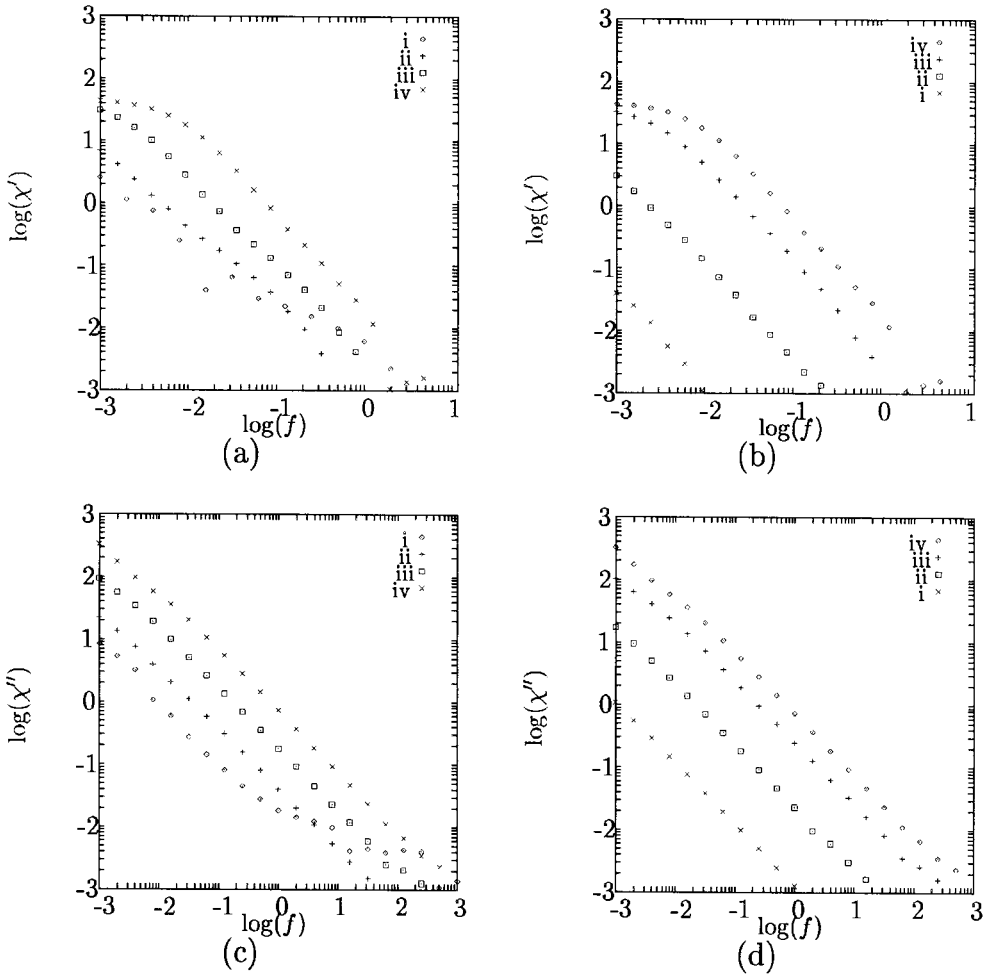

Figure 2. Real ((a), (b)) and imaginary ((c), (d)) parts of the dielectric susceptibility of sample 1. Up ((a) and (c)) and down ((b) and (d)) measurements as functions of frequency before the master curve shifts. The labels (i), (ii), (iii) and (iv) represent 30, 60, 90 and 120 °C, respectively, which are the temperature values at which the measurements were carried out.

The master curve shifts made it easier to observe the dielectric behaviour, since now the number of data points was larger and the frequency range was wider. The master curves of the up and down measurements were similar. The real parts of the susceptibilities, $\chi'(\omega)$, increased with decreasing angular frequency, thus showing dipolar relaxation phenomena. The relaxation in both curves may be explained as Maxwell–Wagner–Sillars polarization arising from the interaction between silica particles and the polymer matrix. The slope of the polarization was proportional to $\chi'(\omega) \propto \omega^{-1.4}$, whereas for a real Debye process $\chi'(\omega) \propto \omega^{-2}$. The static susceptibilities, χ_s, of the sample were around 39.5 and 38.5 for temperatures going up and going down, respectively.

The imaginary parts of the susceptibilities, $\chi''(\omega)$, were parallel to each other and increased towards the lower frequencies. The only difference between them was that they were not at the same angular frequency. The curve of the down measurement was shifted to lower

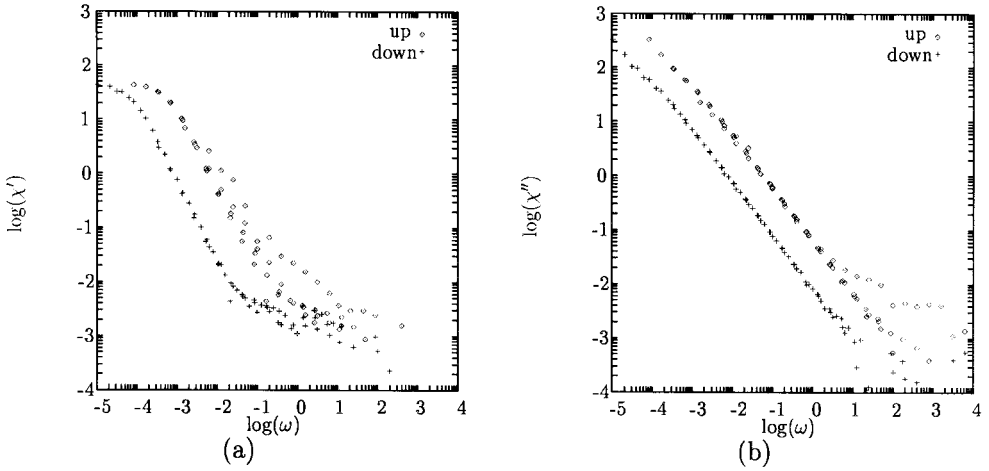

Figure 3. Real (a) and imaginary (b) parts of the master curves for sample 1 from up and down measurements.

frequencies. Although there was a visible dipolar relaxation in the real parts, which should also be seen in the imaginary parts as loss peaks, such behaviour was not observed. The slopes $(\tan(\log \chi''/\log \omega)$ of the imaginary parts were -1, or in other words $\chi \sim (\mathrm{i}\omega)^{-1}$, showing dominating dc conduction behaviour (equation (4)). The differences between the $\chi''(\omega)$ curves for up and down measurements indicate that the available charge carriers either become less mobile or their concentration is lower in the temperature down measurement.

The real and imaginary parts of the master curves were shifted separately. However, the shifting factors, A, were similar. Therefore, an average of the shifting values was used to calculate the activation energies, W, as shown in the Arrhenius plot in figure 4. It was observed

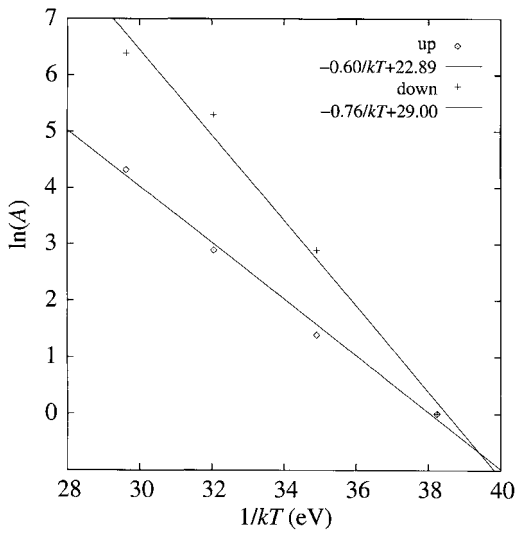

Figure 4. The Arrhenius plot of the angular frequency shift, A, for χ^* for up and down measurements on sample 1.

that polarization and conduction processes were of the Arrhenius type for both measurements. However, the values of the activation energies, W, were different, 0.60 and 0.76 eV for the up and down measurements, respectively.

4.2. The system with 25% of ATH

On adding 50 phr ATH to the basic elastomer, the permittivity values at higher frequencies, ε_{hf}, calculated from up and down measurements were 2.73 and 2.71, respectively, lower than for the sample without any filler. This could be due to the diminishing of high-frequency relaxations caused by a shifting outside the experimental window or else due to the responses contributing to ε_{hf} for sample 1 being pushed to lower frequencies.

There were no visible relaxation behaviours as for sample 1 in the real parts of the responses. The previous relaxation in the material either diminished or moved to lower frequencies with the addition of filler. Moreover, the slopes of the imaginary parts were not -1, i.e. did not show dc conduction contributions as for the previous sample. Thus, the addition of a small amount of filler not only changed the polarization process but changed the conduction mechanism, as well.

The shape of the master curves showed a low-frequency dispersion, where the real and imaginary parts increased towards lower frequencies with a power-law behaviour, $\chi \propto (\mathrm{i}\omega)^a$ where $0 < a < 1$. They were not easy to explain with only one straight line (power-law behaviour) in the log–log plots. Therefore, either two or three different low-frequency dispersions were assumed for the appropriate frequency regions of the spectra. The critical frequencies ($\omega_{c'}$ and $\omega_{c''}$) were assigned when the response changed its inclination, or, in other words, when it was at the knee point in the curve.

The real part of the up master curve was interpreted in terms of two power laws where the critical frequency, $\omega_{c'}$, was at 0.0001 Hz. The exponent of the power laws at low frequencies ($\omega < \omega_{c'}$) was -0.93 and at high frequencies $\omega_{c'} > \omega_{c'}$ it was -0.48. Although these were the values for the two power-law behaviours for the up measurement, the real part of the down measurement did not show such a behaviour. Three power laws were used to fit the response. The two critical frequencies were $\omega_{c'_1} = 0.0002$ Hz and $\omega_{c'_2} = 0.1$ Hz, respectively. At lower frequencies ($\omega < 0.0002$ Hz), the exponent of the power law was lower than that of the up measurement and was -0.87. It was -0.66 between the two critical frequencies. And finally, at higher frequencies ($\omega > 0.1$ Hz) it was -0.40.

Three-power-law behaviour was used to interpret the imaginary parts of the susceptibilities, $\chi''(\omega)$. First, unlike the real part of the up measurement, the imaginary part of the curve had two distinct critical frequencies, $\omega_{c''_1} = 0.001$ Hz and $\omega_{c''_2} = 10$ Hz. The exponent values for the three frequency regions in which $\omega < \omega_{c''_1}$, $\omega_{c''_1} < \omega < \omega_{c''_2}$ and $\omega > \omega_{c''_2}$ were -0.94, -0.51 and -0.10, respectively. Although the exponent on the low-frequency side of the response is close to -1 showing a dc conduction contribution, it was similar to the exponent of the power law of the real part in the same frequency region. This proved the existence of a strong low-frequency dispersion [4]. Moreover, the exponent was also similar in the $\omega_{c''_1} < \omega < \omega_{c''_2}$ regime. It was not possible to conclude anything for the $\omega > \omega_{c''}$ region, since there were not enough $\chi'(\omega)$ data points available.

The imaginary part of the down measurement also showed a behaviour similar to that of the imaginary part of the up measurement. The critical frequencies, ω_c, were the same, $\omega_{c''_1} = 0.001$ Hz and $\omega_{c''_2} = 10$ Hz; however, the exponent values were different. They were -0.88, -0.55 and -0.10 for the frequency regions $\omega < \omega_{c''_1}$, $\omega_{c''_1} < \omega < \omega_{c''_2}$ and $\omega > \omega_{c''_2}$. In contrast to the case for the real and imaginary parts of the up measurement, only the lowest-frequency region ($\omega < \omega_{c''_1}$) of the exponents was close to the exponent value of the real part

of the down curve in the same frequency region. This proved that at frequencies lower than $\omega_{c_1''}$, the material showed a low-frequency dispersion behaviour. However, the exponent in the same regime in the up measurements was higher. Therefore, the charge carriers either became less mobile or else the hopping energy between the sites increased.

In the intermediate-frequency region, $\omega_{c_1''} < \omega < \omega_{c_2''}$, there was no similarity between the exponent values calculated for real and imaginary parts of the down measurements. This indicated that another mechanism besides the low-frequency dispersion was operating in the intermediate-frequency region. Moreover, unlike for the previous sample, the loss values were higher on the high-frequency side of the spectrum.

Arrhenius-type processes were observed. Unlike for sample 1, the activation energies, W, were similar. They were 0.84 and 0.77 eV for the up and down measurements, respectively.

4.3. The system with 33% of ATH

When the concentration of ATH was increased to 33%, the permittivity values of the sample at higher frequencies, ε_{hf}, were 3.29 and 3.26 for the up and down measurements, respectively. The master curves are presented in figure 5. Both real and imaginary parts of the responses were shifted on top of each other. However, the only difference was a little hump between 0.01 and 0.1 Hz in the real part of the up measurement. The effect of the hump was also visible in the imaginary part where the loss values of up measurements were higher than those of the down measurements.

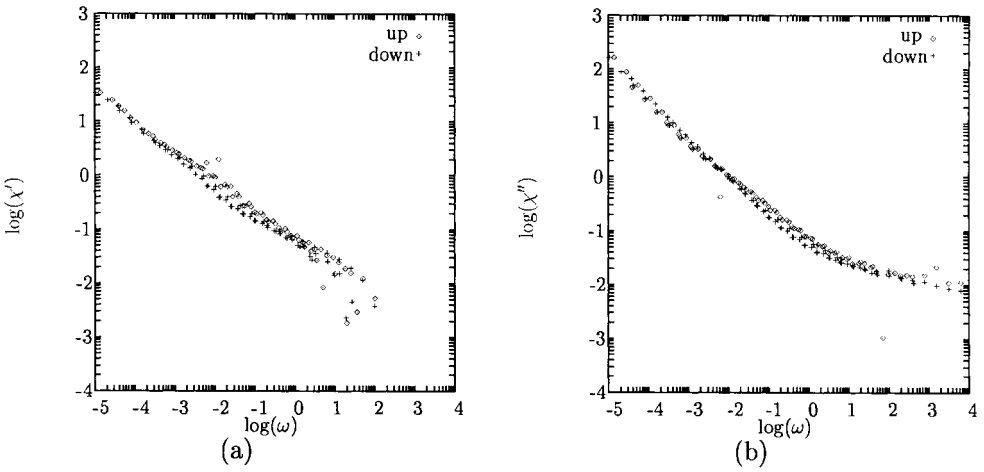

Figure 5. Master curves for sample 3. Real (a) and imaginary (b) parts of the master curves calculated from up and down measurements.

To begin with, the real part of the up master curve showed two-power-law behaviour; the critical frequency, $\omega_{c'}$, was 0.002 Hz. The values of the power-law exponents were -0.73 and -0.47 for $\omega < \omega_{c'}$ and $\omega > \omega_{c'}$, respectively. The real part of the down curve also showed a similar behaviour with $\omega_{c'} = 0.1$ Hz. The exponent values were different to the values for the up master curve and they were -0.61 and -0.34 for the two regimes in which $\omega < \omega_{c'}$ and $\omega > \omega_{c'}$, respectively.

Additionally, the imaginary parts of both the up and down measurements have shown three significant areas with different critical frequencies, $\omega_{c''}$. The critical frequencies of the up curve were $\omega_{c_1''} = 0.001$ Hz and $\omega_{c_2''} = 10$ Hz. The slopes of the log–log straight lines

were -0.91, -0.47 and -0.06 for frequency values $\omega < \omega_{c_1''}$, $\omega_{c_1''} < \omega < \omega_{c_2''}$ and $\omega > \omega_{c_2''}$, respectively. None of these exponents were similar to that of the real part of the curve. One of the reasons for this could be the contribution of dc conduction to the low-frequency region ($\omega < \omega_{c_1''}$), where the exponent value of the power law was close to -1. If the frequencies between 0.001 and 10 Hz are taken into consideration, then, as mentioned before, there is a visible hump which indicated a dipolar relaxation. Thus, the response in this region can be explained by the superposition of a low-frequency dispersion with a dipolar relaxation.

The imaginary part of the down measurement had lower exponent values than that of the up measurements. The critical frequencies were $\omega_{c_1''} = 0.001$ Hz and $\omega_{c_2''} = 2$ Hz. The power-law exponents were -0.81, -0.65 and -0.16 for frequencies $\omega < \omega_{c_1''}$, $\omega_{c_1''} < \omega < \omega_{c_2''}$ and $\omega > \omega_{c_2''}$. Unlike that for the imaginary part of the up measurements, the exponent value at low frequencies ($\omega < \omega_{c_1''}$) was lower. In addition, the exponent of the real part was lower than that of the imaginary part in this region, indicating that there was also a dc conduction contribution as in the up measurements.

Furthermore, in the intermediate-frequency region $\omega_{c_1''} < \omega < \omega_{c_2''}$ the exponents of the power laws of the real and imaginary parts were close to each other. This showed that the dipolar polarization process that was present in the up measurements either diminished or else its relaxation time changed. Finally, the activation energies calculated from Arrhenius plots (figure 6) were approximately the same, 0.78 and 0.82 for the up and down measurements, respectively.

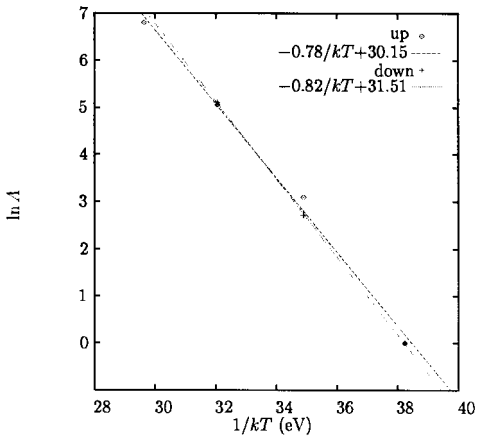

Figure 6. The Arrhenius plot of the angular frequency shift, A, for χ^* for up and down measurements on sample 3.

4.4. The system with 50% of ATH

The dielectric permittivities at higher frequencies, ε_{hf}, obtained from the temperature up and down measurements were 3.45 and 3.48, respectively, as the sample was half elastomer and half ATH. The up and down master curves showed similar characteristics. The difference between them was, as for the sample without any filler material, that the down measurement shifted to lower frequencies. Again, as for the previous sample containing 33% filler, there were humps in the real parts of the curves between 0.001 and 1 Hz; furthermore, the hump of the up measurement was more pronounced, and was also observed in the imaginary parts of the curves.

First, it was possible to interpret the real parts of the up and down measurements as two-power-law behaviour. The critical frequency, $\omega_{c'}$, of the former was 0.001 Hz. The exponent values of the two power laws for $\omega < \omega_{c'}$ and $\omega > \omega_{c'}$ were -0.52 and -0.45, respectively. The critical frequency of the real part of the down measurement was $\omega_{c'} = 0.008$ Hz and the exponents were -0.52 and -0.40 for frequencies $\omega < \omega_{c'}$ and $\omega > \omega_{c'}$, respectively. However, the small difference in the real parts between the two frequency regions could be due to the visible dipolar relaxation hump, which was not taken into account in fitting the power laws. Just as for sample 1, the shapes of the curves were similar, which was also supported by the similar exponent values.

Second, the imaginary parts of the curves were also parallel to each other. Unlike the case for the real parts of the responses, three power laws were used to describe the behaviour of the curves. The critical frequencies of the imaginary part of the up master curve were $\omega_{c_1''} = 0.008$ Hz and $\omega_{c_2''} = 70$ Hz. The exponents of the power laws were -0.72, -0.47 and -0.15 for frequencies $\omega < \omega_{c_1''}$, $\omega_{c_1''} < \omega < \omega_{c_2''}$ and $\omega > \omega_{c_2''}$, respectively. Again as for the sample with a 33% ATH concentration (sample 3), the low-frequency edge of the imaginary part of the up measurement had a steeper slope than the real part had, indicating the contribution of the dc conduction. The intermediate-frequency region, $\omega_{c_1''} < \omega < \omega_{c_2''}$, of the imaginary part and the real part of the up curve were taken into account, and the exponent values were close to each other, thus emphasizing low-frequency dispersion contributions.

Moreover, the imaginary part of the down measurement also had two critical frequencies, and they were $\omega_{c_1''} = 0.001$ Hz and $\omega_{c_2''} = 10$ Hz. The exponents were -0.72, -0.51 and -0.13 in the frequency regimes $\omega < \omega_{c_1''}$, $\omega_{c_1''} < \omega < \omega_{c_2''}$ and $\omega > \omega_{c_2''}$, respectively. These exponential values were very close to those in the up measurements, something which was not observed for the previous samples. First, by comparing the real and imaginary parts of the down measurements, it was again observed that there was a dc conduction contribution. Next, as in the up measurement, the difference between the exponent values of the high-frequency side ($\omega > \omega_c$) of the real part and the intermediate-frequency region ($\omega_{c_1''} < \omega < \omega_{c_2''}$) of the imaginary part of the down curve could be due to the dipolar relaxation that was visible in the response. There were not that many changes between the up and down measurements, if the exponents of the power laws were taken into consideration.

The sample was more reliable and the shapes of the master curves were similar; however, the activation energies calculated from the master curve shifts were 0.69 and 0.78 for the up and down measurements.

4.5. The system with 60% of ATH

The average dielectric permittivity values at high frequencies, ε_{hf}, were 3.88 and 3.90 from the up and down measurements. The permittivities were comparable to those for the sample without any filler. The master curves of the up and down measurements did not shift on top of each other. Moreover, they showed a low-frequency dispersion relation. A little hump was visible in the real part of the up measurement between frequencies 0.002 and 1 Hz. The hump was not visible in the down measurements.

The power-law analysis of the real parts of the master curves has shown different behaviour. It was enough to fit just one power law to the real part of the down measurement; on the other hand, the real part of the up measurement was modelled by three power laws. Therefore, the frequency region was divided into three regions with the critical frequencies $\omega_{c_1'} = 0.002$ Hz and $\omega_{c_2'} = 1$ Hz. The exponents of the power laws in the regions were -0.47, -0.31 and -0.50 for the $\omega < \omega_{c_1'}$, $\omega_{c_1'} < \omega < \omega_{c_2'}$ and $\omega > \omega_{c_2'}$ regimes, respectively. Since several low-frequency dispersion phenomena, $\chi^*(\omega) \propto \sum(\mathrm{i}\omega)^{a_i}$, are considered, a decrease in the

exponents, a_i, is to be expected with decreasing frequency. Therefore, the exponent value (-0.50) at high frequencies proved the presence of the dipolar relaxation in the middle of the frequency range considered, as mentioned above. Additionally, the real part of the down measurement did not have any critical frequency, $\omega_{c'}$. It was a straight line in the log–log plot with the slope -0.37.

The imaginary parts of the curves have shown different power-law behaviour. First, the imaginary part of the up curve had its critical frequency at $\omega_{c''} = 0.02$ Hz, The slopes of the log–log lines used to interpret the curve below and above the critical frequency, $\omega_{c''}$, were -0.83 and -0.32. These results have shown that there was a dc conduction contribution to the imaginary part of the up master curve, since the exponent value of the real part was not similar to the one for the low-frequency side of the spectrum. At the same time, the exponents of the power laws of the real and imaginary parts in the frequency region $0.002 < \omega < 1$ Hz were close enough to show a low-frequency dispersion. Finally, the dipolar relaxation was not significant in the imaginary part of the up measurement.

The imaginary part of the down measurement had two critical frequencies, $\omega_{c''_1} = 0.001$ Hz and $\omega_{c''_2} = 100$ Hz. Accordingly, the exponents were -0.87, -0.37 and -0.11 for the frequency regimes $\omega < \omega_{c''_1}$, $\omega_{c''_1} < \omega < \omega_{c''_2}$ and $\omega > \omega_{c''_2}$, respectively. In the down measurement, the dc conduction and low-frequency dispersion were much more clearly separated at $\omega = 0.001$ Hz, although the low-frequency dispersion in the high-frequency part of the imaginary part was not visible in the real part. This could be due to the way in which ε_{hf} was calculated. Since the exponent of the power law (-0.11) was close to 0 (the dielectric permittivity, $\varepsilon'(f)$, was nearly flat), it could have been subtracted from ε' for the down measurement.

If the behaviour at low frequencies is taken into consideration, the exponents of the power laws of the imaginary parts indicated that dc conduction decreases in the down measurement. The activation energies are 0.62 and 0.85 eV, respectively.

4.6. The system with 67% of ATH

The dielectric permittivities of the sample at higher frequency values, ε_{hf}, were 4.42 and 4.45 for the up and down measurements, respectively. Low-frequency dispersions were observed from the master curves where the real and imaginary parts of the curves increased, once again, towards the low frequencies. The shifts of the master curves were not on top of each other and the separation of the curves became larger.

The real part of the up measurement had a critical frequency, $\omega_{c'}$ at 0.001 Hz. The power-law behaviour for frequencies lower than $\omega_{c'}$ had -0.55 as the exponent. At frequencies higher than $\omega_{c'}$ this value was -0.36. The real part of the down measurement did not have a significant critical frequency; however, the slope of the curve changed at around 0.000 03 Hz. Since this frequency value was really low and the number of data points available was low, the value of the exponent of the power law used to fit the data was not calculated. Thus, only one power law was considered, and its exponent was -0.36, which was similar to the exponent value for the up measurement in the high-frequency region.

The imaginary parts of the master curves were modelled by two and three power laws for the up and down measurements, respectively. The imaginary part of the up measurement started to increase up to the critical frequency $\omega_{c''} = 0.01$ Hz with a slope value of -0.35. This value supported the low-frequency dispersion behaviour because it was close to the exponent value of the real part of the same measurement. However, the imaginary part changed its inclination to -0.92 after $\omega_{c''}$, showing a strong dc conduction contribution. At the same time, the three frequency regions of the imaginary part of the down measurement were separated

by the critical frequencies $\omega_{c_1''} = 0.001$ Hz and $\omega_{c_1''} = 20$ Hz. The corresponding exponent values of the power laws were -0.83, -0.38 and -0.16, respectively. Comparing the power-law exponent of χ'' at low frequencies with that of the real part, χ'' has a higher value, thus showing the contribution of dc conduction. At frequencies lower than $\omega_{c_1''}$, the exponents of the real and imaginary parts confirmed a low-frequency dispersion. The power-law behaviour was not visible in the real part of the down curve over a high-frequency region as for the previous sample; it could be lost in the susceptibility calculations owing to the low slope value.

Again, as for the previous samples, the dc conduction contribution to the losses decreased in the down measurements. The activation energies calculated from the master curve shifts were 0.64 and 0.88 for the up and down measurements, respectively.

4.7. The system with 71% of ATH

This system had the highest ATH concentration. The dielectric permittivity values at higher frequencies, ε_{hf}, were 4.54 and 4.55 for the up and down measurements, respectively. The master curves once again showed low-frequency dispersions (figure 7), and did not shift on top of each other. Moreover, the spread between the up and down curves was the largest of all. The shapes of the curves were not the same: first of all, the slopes of the real parts of the master curves were different. The real part of the up measurement had a steeper slope than that of the down measurement. This was also the case for the imaginary parts of the curves.

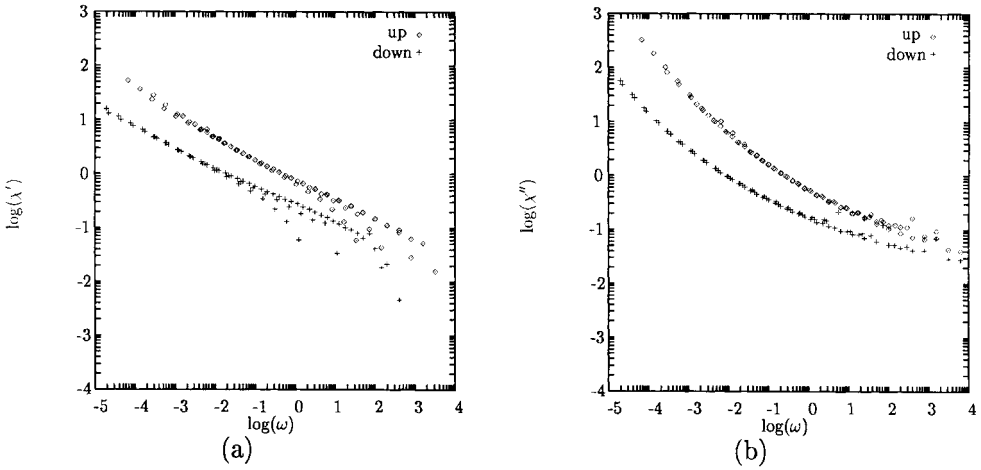

Figure 7. Master curves for sample 7. Real (a) and imaginary (b) parts of the master curves calculated from up and down measurements.

There were no signs of dipolar relaxations in the master curves, unlike for the other samples. The power-law exponents of the real parts were -0.43 and -0.35 for the up and down measurements, respectively. Although it was possible to explain the real parts with one power law, this was not the case for the imaginary parts: they were divided into three frequency regions. Starting with the imaginary part of the up measurement, the critical frequencies were $\omega_{c_1''} = 0.02$ Hz and $\omega_{c_2''} = 100$ Hz. The power-law exponents were -0.89, -0.45 and -0.20 for the frequency regions $\omega < \omega_{c_1''}$, $\omega_{c_1''} < \omega < \omega_{c_2''}$ and $\omega > \omega_{c_2''}$, respectively. Again, the intermediate-frequency-region value of the exponent was close to that of the real part of the measurement, thus proving a low-frequency dispersion. That for the low-frequency side was

governed by the dc conduction contribution and it was close to -1. Furthermore, a small low-frequency dispersion at high frequencies was not visible in the real part because of its small contribution.

In the same way, the imaginary part of the down measurement had two frequencies: $\omega_{c_1''} = 0.002$ Hz and $\omega_{c_2''} = 10$ Hz. Although the critical frequencies have shown resemblances to those of the up measurements, the exponent values of the three power laws were not the same. They were -0.73, -0.36 and -0.18 for the regions $\omega < \omega_{c_1''}$, $\omega_{c_1''} < \omega < \omega_{c_2''}$ and $\omega > \omega_{c_2''}$, respectively. The real and imaginary parts of the down measurements also proved that there were contributions from the low-frequency dispersion at frequencies $\omega_{c_1''} < \omega < \omega_{c_2''}$, and a dc conduction at frequencies $\omega < \omega_{c_1''}$.

As usual, both the dc conductivity and low-frequency contributions decreased in the down measurements. Arrhenius plots of the measurements for temperatures going up and down are presented in figure 8. The activation energies were 0.53 and 0.91 eV.

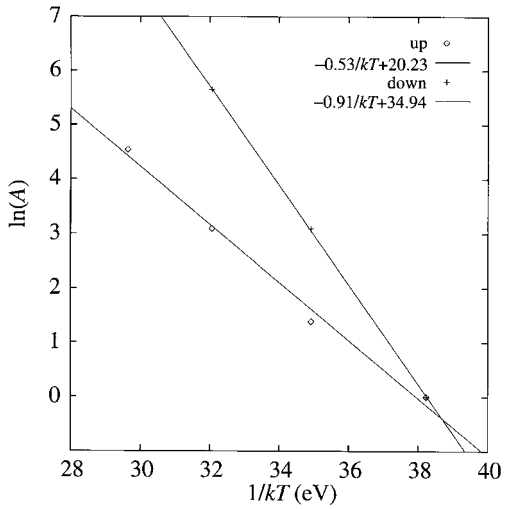

Figure 8. The Arrhenius plot of the angular frequency shift, A, for χ^* for up and down measurements on sample 7.

5. Discussion

5.1. Effects of filler on dielectric permittivities at higher frequencies

The dielectric permittivity values of the samples at higher frequencies, ε_{hf}, as a function of the ATH concentration, q, are presented in figure 9. The average values of ε_{hf} were calculated using equation (9). In figure 9, the values are presented with their standard deviations by separating them at the concentration axis to make the data points more visible. Without any filler, the value of ε_{hf} was higher than for the samples with lower filler content. This could have been due to a change in polarization of the polymer molecules at frequencies higher than 1 kHz. Adding a small amount of filler could decrease the mobility of polymer chains (shifting the spectra to lower frequencies), which, in the filled state, contribute to the polarization in this frequency region. A similar decrease could also be expected if the permittivity of the ATH was lower than that of the base polymer. Moreover, assuming the exponents of low-frequency dispersions to be the same for the unfilled and filled samples, and the low-frequency dispersion

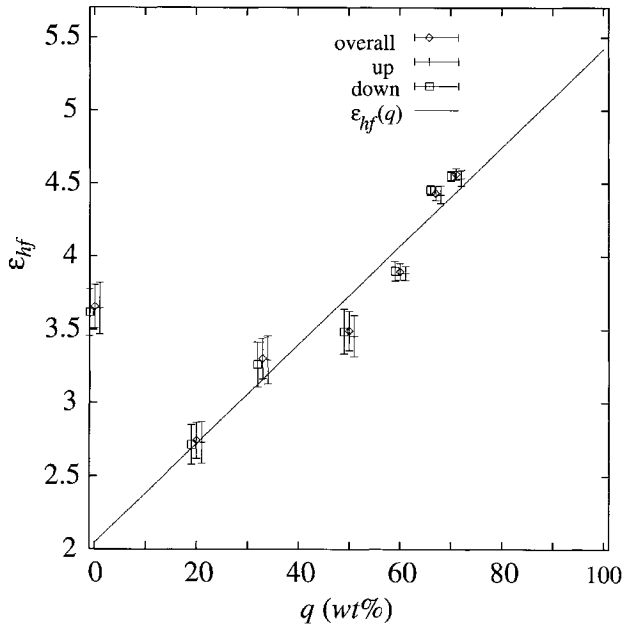

Figure 9. Dielectric permittivity at higher frequencies as a function of ATH concentration in wt% where $\varepsilon_{hf}(q) = 0.0337\,q + 2.0477$.

parameter, ς, of the unfilled sample to be larger than that of the filled one, the low-frequency contributions will also give a higher ε_{hf}-value for the unfilled sample.

After adding 20 wt% of filler, ε_{hf} decreased to the lowest level. It started to increase linearly again with further addition of filler to the rubber, thus proving that the permittivity of the ATH must have been higher than the permittivity of the base polymer. This effect cannot be explained by the theory of binary dielectric mixtures [1]. One of the interesting results was that a composite sample with ~60 wt% had an ε_{hf}-value similar to that of the unfilled material. Data on dielectric properties of ATH are not available in the literature, but if one assumes that the linear dependence is also obeyed for higher concentrations, this leads to the permittivity of ATH, $\varepsilon_{hf_{ATH}} = 5.42$.

5.2. Master curves

The shape of the master curves changed drastically with the addition of filler. Without any filler, there were two clear processes, i.e. dipolar relaxation and dc conduction. The addition of filler altered the behaviour of the master curves. For the samples with filler, the real and imaginary parts of the master curves were nearly parallel to each other, thus showing a low-frequency dispersion. The contribution of the low-frequency dispersion ($\chi^* \propto (\mathrm{i}\omega)^a$) was the strongest for the sample with 20% filler with the power-law exponent $a = -0.93$. Additionally, the increase of ATH concentration decreased the contribution of the strong low-frequency dispersion. At the same time, there was no visible dc conduction for samples with less filler; however, the samples with higher filler content had dc conduction contributions in their responses at low frequencies. The dipolar relaxation that was significant for the real part of the sample without any filler was not observable for the samples with filler. In contrast to this dipolar relaxation, there were little humps in the frequency range $0.001 < \omega < 10$ Hz

in the responses of the samples with filler, with the exception of the two highest-filler-content materials (samples 6 and 7).

For all samples, the real parts of the responses higher than 100 Hz were not present due to the subtraction of ε_{hf} from the data points to obtain the susceptibilities, $\chi'(\omega)$. Therefore, comparisons of the real and imaginary parts of the master curves were not possible and the information about the small contributions of the low-frequency dispersion in these regions was lost.

One of the interesting results from the up and down measurements was that there were significant differences between the master curves. Only the up and down master curves for samples 2 and 3 fell on top of each other (figure 5). For all the other master curves, the down curve was shifted to lower frequencies. This could be due to the electrical history of the samples, since the thermal history of the samples—i.e. in the sample preparations they were heated up to 150 °C—involved a higher temperature value than the highest measurement temperature, 120 °C. During the up measurements, either the concentrations of the charge carriers or their mobilities were altered. Therefore, the possible sites which the charge carriers can choose in the hopping mechanisms were fewer, or else the frequency of hopping between the sites was lower for the down measurements.

Moreover, the humps that were present in the up measurements were not visible in the down measurements. This could, again, be due to the electrical history of the samples. On the other hand, the hump could be pushed to lower frequencies in the down measurements. If one considers the hopping between two possible sites, which is observed as a dipolar relaxation, the sites contributing to the hump in the dipolar relaxation might be filled after the up measurements.

5.3. Activation energies

Filler content influenced the activation energies, W, of the dielectric processes. In table 2, the activation energies W are presented. If the up measurements are taken into account, then the activation energy of the first sample is $W = 0.60$ eV. The addition of the 20 wt% filler increased the activation energy to $W = 0.84$ eV. However, further increase of the filler decreased W significantly, down to 0.53 eV. On the other hand, the activation energies of the down measurements were close to each other: $0.76 < W < 0.84$, with a tendency to increase with higher ATH concentration. Only samples 2 and 3 had close activation energies

Table 2. Sample numbers, losses at angular frequencies 0.0001 Hz and 100 Hz, activation energies and the relative permittivity at higher frequencies. Activation energies are obtained using master curve shifts. The arrows represent the temperature going up (↗) and down (↘) in the measurements.

	Losses (χ'')						
	at 0.1 kHz		at 0.1 mHz		W (eV)		
Sample	↗	↘	↗	↘	↗	↘	ε_{hf}
1	0.00	0.00	160	50.2	0.60	0.76	3.66 ± 0.15
2	0.01	0.01	7.9	16.0	0.84	0.77	2.74 ± 0.12
3	0.01	0.02	27.0	26.7	0.78	0.82	3.30 ± 0.14
4	0.03	0.02	25.0	16.4	0.69	0.78	3.49 ± 0.13
5	0.07	0.04	82.0	17.7	0.62	0.85	3.90 ± 0.06
6	0.13	0.06	92.0	21.9	0.64	0.88	4.44 ± 0.05
7	0.12	0.06	240	18.6	0.53	0.91	4.54 ± 0.04

as calculated from the up and down measurements. The master curves of the samples were also shifted on top of each other. Another interesting result was that these two samples had similar activation energies. One can conclude that there were not that many differences between the outcomes for 20 wt% and 30 wt% filler content, which are around the percolation threshold. At the same time, samples 6 and 7 had only 4 wt% filler difference and their activation energies derived from the up measurements were not similar.

6. Modelling dielectric susceptibilities

The master curves obtained from frequency shifting were smoothed using a nonparametric local averaging technique [32]. The differences between the data points and the smoothed curve were assigned as errors ($\epsilon_{\chi'}$ and $\epsilon_{\chi''}$), and since the figures are plotted in log–log coordinates, the error bars appear larger at the lower limits than they would do in linear coordinates. The dielectric susceptibilities were then modelled by using three contributions, i.e. Havriliak–Negami dipolar relaxation, dc conduction and low-frequency dispersion (hopping conduction) as in equation (6). The equation was separated into real and imaginary parts:

$$\begin{aligned} \chi'_m &= \frac{\chi_s \cos(C)}{(A^2+B^2)^{\beta/2}} + \frac{\varsigma}{\varepsilon_0 \omega^\gamma \cos(\gamma\pi/2)} \\ \chi''_m &= \frac{\chi_s \sin(C)}{(A^2+B^2)^{\beta/2}} + \frac{\sigma_{dc}}{\varepsilon_0 \omega} + \frac{\varsigma}{\varepsilon_0 \omega^\gamma \sin(\gamma\pi/2)} \end{aligned} \tag{10}$$

where χ'_m and χ''_m are the modelled susceptibility values and A, B and C are

$$\begin{aligned} A &= 1 + (\omega\tau)^\alpha \cos(\alpha\pi/2) \\ B &= (\omega\tau)^\alpha \sin(\alpha\pi/2) \\ C &= \beta \tan^{-1}(B/A). \end{aligned} \tag{11}$$

Then, a nonlinear least-squares fitting method was used to fit the master curves [24]. The method was applied for both real and imaginary parts of the data, χ'_e and χ''_e, simultaneously. The χ^2-test (denoted by Θ_χ) was used for error minimization to determine the goodness (agreement) of the fits:

$$\Theta_\chi = \sum \left[\frac{(\chi'_e - \chi'_m)^2}{\epsilon_{\chi'_e}} + \frac{(\chi''_e - \chi''_m)^2}{\epsilon_{\chi''_e}} \right]. \tag{12}$$

Results of the fitting are presented in table 3 and figures 10, 11 and 12 which show the fits and master curves with error bars (ϵ_χ). Cross correlations between the adjustable parameters were checked and there were no correlations between them [33].

6.1. Dipolar relaxations

The fitting parameters for the Havriliak–Negami dipolar relaxation changed drastically with the ATH concentration (table 3). First, the up measurement of the sample without any filler material showed near-Debye-like behaviour with $\alpha = 0.99$ and $\beta = 0.98$. The static susceptibility, χ_s, and the relaxation time, τ, were 39.5 and 1600 s, respectively. These values for the down measurements were slightly different; the relaxation was closer to Debye-like dipolar relaxation, $\alpha = 0.99$ and $\beta = 0.99$, and the static susceptibility, χ_s, was lower than the up measurement. The most significant difference was in the relaxation time, τ. The dipolar relaxation was slower in the second part of the measurement, $\ln \tau \sim 7.4$ s. The relaxation was also visible in the imaginary part of the master curves as a hump addition to the dc conduction

Table 3. Sample numbers and fitting parameters for the Havriliak–Negami dipolar relaxation, dc and hopping conductions in equation (6).

Sample No	α	β	χ_s	$\ln(\tau)$	$\log(\sigma_{dc})$	$\log(\varsigma)$	γ
Up							
1	0.99	0.98	39.5	7.4	−12.7	−13.7	0.05
2	0.81	0.60	1.1	7.0	−14.9	−13.3	0.84
3	0.76	0.70	1.2	5.1	−14.0	−12.8	0.79
4	0.80	0.60	1.3	4.0	−13.9	−12.3	0.62
5	0.79	0.52	1.1	2.2	−13.4	−11.8	0.51
6	0.78	0.49	1.1	1.9	−13.3	−11.6	0.55
7	0.78	0.49	0.3	−1.6	−12.8	−11.2	0.47
Down							
1	0.99	0.99	38.5	9.2	−13.5	−13.7	0.05
2	0.82	0.61	0.9	6.8	−14.9	−13.2	0.84
3	0.76	0.70	0.0	1.2	−13.9	−12.3	0.62
4	0.80	0.70	0.1	−0.5	−14.4	−12.1	0.55
5	0.79	0.51	0.3	1.8	−14.2	−11.8	0.46
6	0.78	0.49	0.3	0.2	−14.1	−11.8	0.50
7	0.78	0.51	0.3	−0.9	−13.7	−11.9	0.52

contribution. This dipolar relaxation mechanism could be from the interface between silica and silicone polymer due to the Maxwell–Wagner–Sillars effect.

Considering the filled samples and starting with the up measurement for the second sample, there was a dipolar relaxation process with a relaxation time, τ, close to that of the unfilled sample. On the other hand, the static susceptibility value, χ_s, of this dipolar relaxation was much lower, $\chi_s = 1.1$. Moreover, not only χ_s, but also the shape of the near-Debye-like behaviour was altered by the presence of the filler: the response curve was broadened, $\alpha = 0.81$ and $\beta = 0.60$. The difference between the master curves for the filled and unfilled samples can be interpreted in two ways. First, the dipolar relaxation could be from the silica–silicone interface with a lower χ_s-value. Second, this could be a new dipolar relaxation and the previous relaxation from the silica–silicone interface could have been pushed to lower frequencies. Finally, the fitting parameters for the down measurements on sample 2 were similar to those for the up measurements. There were no pronounced differences as for sample 1.

For samples 3–6, the master curves for the up measurements had dipolar relaxation similar to that for sample 2. However, the relaxation times, τ, were moved to higher frequencies or, in other words, became faster with the further addition of filler. The shapes of the relaxations were also broadened (β became smaller). If the down measurements are taken into consideration, the dipolar relaxation processes are not that significant. Their static dielectric susceptibilities, χ_s, are lower than for the up measurements. Furthermore, the sample with the highest ATH concentration (sample 7) also shows behaviour in the relaxation process similar to those of the other filled samples. The relaxation time, τ, of the polarization moves to higher frequencies, $\ln \tau \sim -1.6$ s (see table 3 and figure 12). Moreover, it has the lowest static dielectric susceptibility, χ_s. The up and down measurements also have fitting parameters similar to those for sample 2.

On the whole, with increasing ATH concentration, a new relaxation process appeared in the experimental window with a much lower static dielectric susceptibility, χ_s, than for the unfilled sample (see table 3). At the same time, the previous relaxation process was either

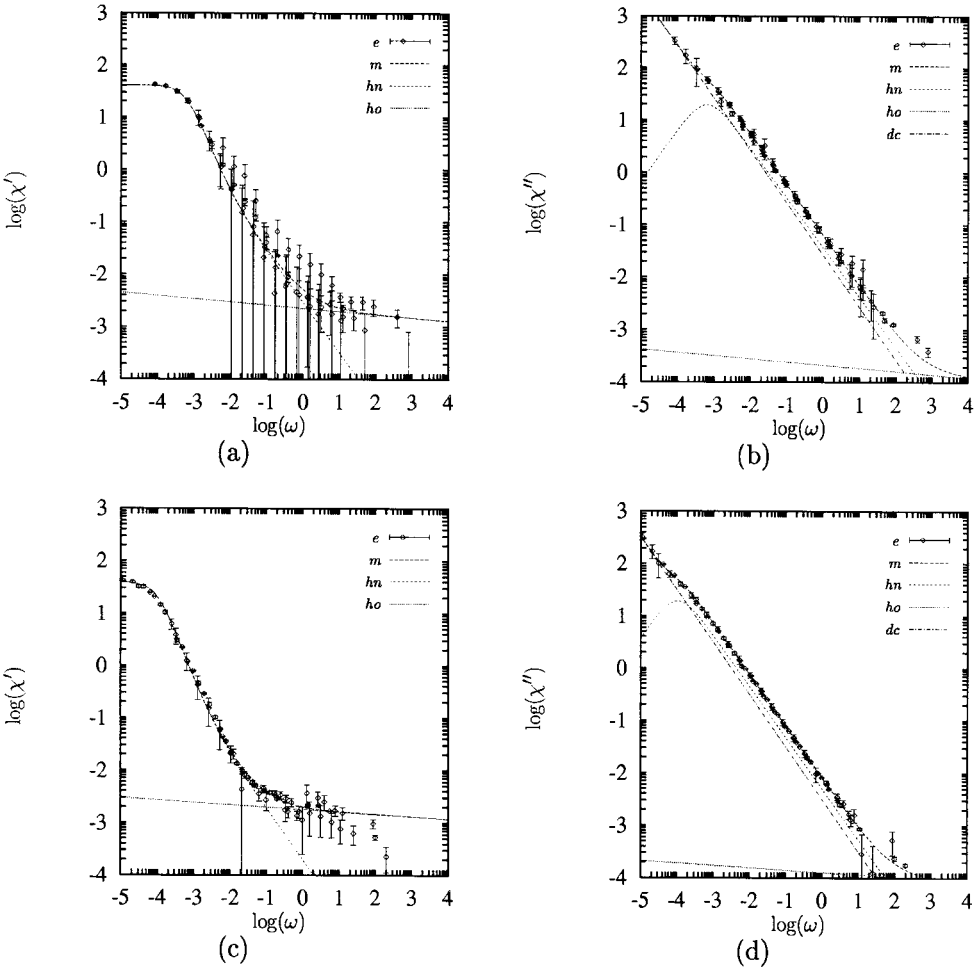

Figure 10. Real ((a) and (c)) and imaginary ((b) and (d)) parts of the dielectric susceptibilities of sample 1 for the up ((a) and (b)) and down ((c) and (d)) measurements. The labels *e*, *m*, *hn*, *ho* and *dc* represent experimental, modelled ($\chi_m = \chi_{hn} + \chi_{ho} + \chi_{dc}$), Havriliak–Negami, hopping conduction and dc conduction contributions, respectively.

pushed out to the left-hand side of the experimental window or diminished. It was not visible. This new relaxation process had a Havriliak–Negami dipolar relaxation shape with α nearly constant for the samples with filler material: about 0.8, and decreasing β with increasing ATH concentration. The sample with the highest ATH concentration had the lowest static susceptibility, χ_s, and the fastest relaxation time, τ. Lastly, the relaxation in filled samples was not that visible in the down measurements.

As a result of the microstructural change of the samples with the addition of the filler, the polymer started to become isolated in small island-like structures and the thickness of the polymer layer on the filler particles was reduced. The islands and the layer thickness then became smaller with the further addition of filler. Thus, the relaxation due to the interface between the filler and the polymer became faster, thus showing an increase in the interface conductivity which could explain the movement of the relaxation to higher frequencies. Moreover, in the down measurements, either the conductivity of the islands and layer or the mobility of the charge carriers was lowered.

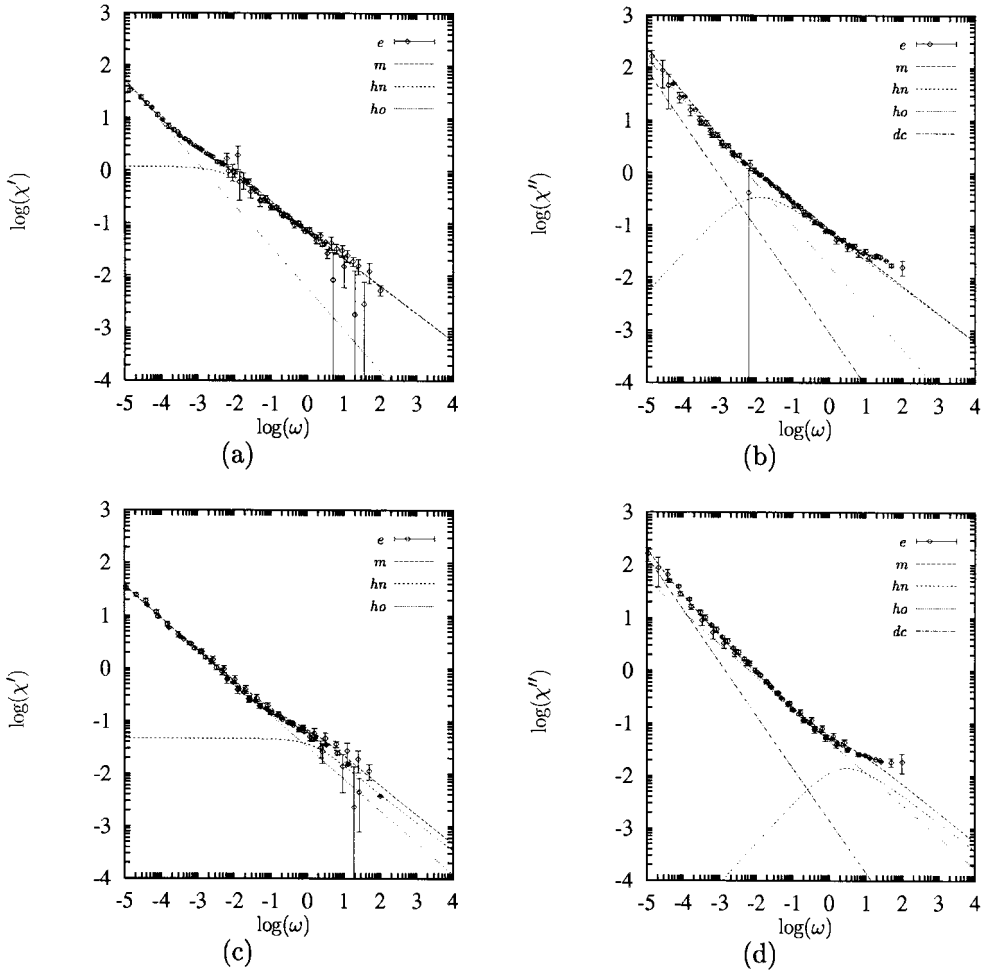

Figure 11. Real ((a) and (c)) and imaginary ((b) and (d)) parts of the dielectric susceptibilities of sample 3 for the up ((a) and (b)) and down ((c) and (d)) measurements. The labels *e*, *m*, *hn*, *ho* and *dc* represent experimental, modelled ($\chi_m = \chi_{hn} + \chi_{ho} + \chi_{dc}$), Havriliak–Negami, hopping conduction and dc conduction contributions, respectively.

6.2. Direct-current conduction and low-frequency dispersion

The fit parameters for dc conduction and hopping conduction are also presented in table 3 and figure 13; all the values are from 30 °C. Looking at the up measurements, it can be observed that the dc conductivity first drops by about two orders of magnitude and then increases again to a value similar to that for the unfilled sample; this is also visible at lower frequencies of the dielectric spectra. On the other hand, if ς is assumed to be the hopping conductivity, it is increased by increasing the ATH concentration (see table 3). The exponent of the hopping conductivity, γ, first shows a strong low-frequency dispersion ($\chi^* \propto (\mathrm{i}\omega)^{-0.84}$) and is decreased by increasing the ATH concentration, thus making the shape of the dielectric responses moderate, $\chi^* \propto (\mathrm{i}\omega)^{-0.47}$. The change of the dc conductivity, σ_{dc}, verifies the assumption of shrinking polymer and the conduction of the interface, as discussed in the previous section.

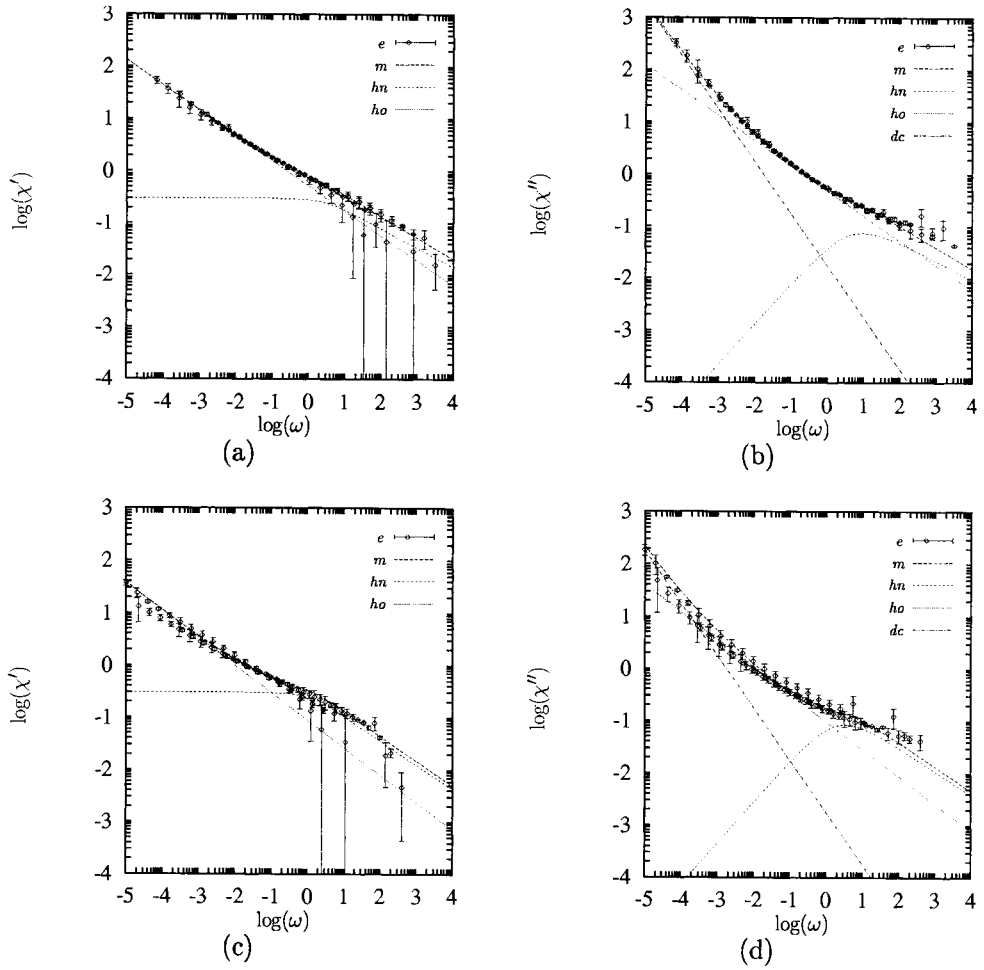

Figure 12. Real ((a) and (c)) and imaginary ((b) and (d)) parts of the dielectric susceptibilities of sample 7 for the up ((a) and (b)) and down ((c) and (d)) measurements. The labels e, m, hn, ho and dc represent experimental, modelled ($\chi_m = \chi_{hn} + \chi_{ho} + \chi_{dc}$), Havriliak–Negami, hopping conduction and dc conduction contributions, respectively.

Comparing the fitting parameters for the up and down measurements, one can see significant changes in the hopping conductivity values, ς, the exponent of the power laws, γ, and the dc conductivity, σ_{dc}. There was no simple relation between the hopping conduction contribution parameters, γ and ς, for the up and down measurements; however, they were close to each other. On the other hand, the dc conductivities, σ_{dc}, obtained from the down measurements were lower than those from the up measurements, except for the two samples—samples 2 and 3—which had similar dc conductivity values in both measurements. The difference between the conductivities of the up and down measurements could be explained by the mobilities of the charge carriers and the electrical history of the samples. The difference between the dc conductivities of the up and down measurements also confirms the previous suggestions regarding relaxation times.

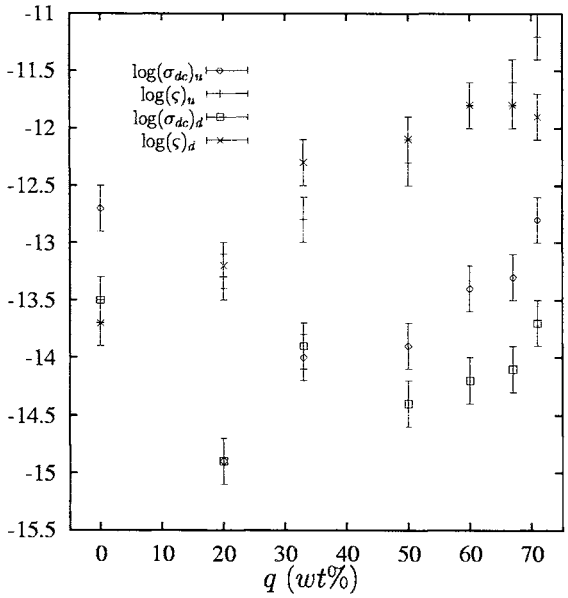

Figure 13. Direct-current and hopping conductivities as a function of the ATH concentration. Subscripts *u* and *d* represent up and down measurements, respectively.

7. Conclusions

Silicone rubber samples with different concentrations of ATH filler show different electrical properties. The contribution from different electrical processes, i.e. dipolar relaxation, dc conduction and low-frequency dispersion (hopping conduction), dominate the properties of the samples, depending on the concentration of the filler. The sample without any filler shows a clear near-Debye-like dipolar relaxation and a strong dc conduction. On the other hand, samples with average filler content exhibit significant low-frequency dispersion, whereas the dipolar relaxation and dc conduction contributions are much weaker in their spectra. However, the further addition of filler causes the dc conduction contribution to increase again. Moreover, in the filled samples a new dipolar relaxation appears with a much lower static dielectric susceptibility than the one for the unfilled samples. This new relaxation moves to higher frequencies with increasing filler content.

The experiments have revealed differences in the dielectric response spectra depending on whether the samples were heated up or cooled down during the measurements. The differences appeared in the position of the spectra on the frequency axis, as well as in the activation energies. The discrepancy was the lowest when the ATH content was moderate (25 and 33%).

During the measurements, at each frequency sweep at a constant temperature, localized states (traps or hopping sites) responsible for the conduction process were filled. Since in the up measurements the following temperature was always higher than the previous one, some of the charge carriers in these localized states were able to discharge or become mobile as for example in the thermally stimulated depolarization current measurement [34]. However, in the down measurement, the charge carriers were frozen in the localized states and obstructed the conduction process. Accordingly, there were discrepancies between the up and down measurements. Therefore, it seems reasonable to believe that the electrical history of the samples was responsible for the discrepancy. If there were any effects from the thermal history,

the master curve approach should have failed; moreover the samples were moulded at 135 °C and cured at 150 °C; both temperature values are higher than the measurement temperatures.

There were no samples with filler content between 0 and 20 wt% in this study. All the samples, even the one without ATH, had filler contents above the percolation threshold. However, if we assume that the silicone elastomer had silica as a matrix material, then the discrepancies between the up and down measurements were lowest when the ATH content was around the percolation threshold (20–33 vol%) which coincides with the model proposed by [21]. Traps decreased the number of charge carriers and their mobility. The fit parameters from the model also confirmed this suggestion.

The dielectric permittivity value for the unfilled sample at high frequencies, ε_{hf}, was higher than that for the filled samples. Considering only the filled samples, it was observed that ε_{hf}-values were proportional to the filler content, yielding $\varepsilon_{hf} \sim 5.4$ for ATH.

Acknowledgments

The support of the Foundation for Strategic Research is gratefully acknowledged. The authors would like to thank ABB Corporate Research for their support in supplying and preparing the materials, and permitting us to use the measurement facilities in Västerås, Sweden. Dr K Dowling and Mr H Hillborg are thanked for their help in the preparing of samples and Drs B Nettelblad, B Mellander and U Gäfvert are also thanked for fruitful discussions.

References

[1] Priou A (ed) 1992 Progress in electromagnetics research *Dielectric Properties of Heterogeneous Materials* (New York: Elsevier)

[2] Landauer R 1978 Electrical conductivity in inhomogeneous media *Electrical Transport and Optical Properties of Inhomogeneous Media (AIP Conf. Proc. vol 40)* ed J C Garland and D B Tanner (New York: American Institute of Physics) pp 2–43

[3] Hale K D 1976 The physical properties of composite materials *J. Mater. Sci.* **11** 2105–41

[4] Jonscher A K 1983 *Dielectric Relaxation in Solids* (London: Chelsea Dielectric)

[5] Maxwell J C 1891 *A Treatise on Electricity and Magnetism* 3rd edn, vol 1 (Oxford: Clarendon) pp 450–64 (reprinted by Dover, New York)

[6] Wagner K W 1914 Erklärunf der dielekrischen Nachwirkungsvorgänge auf Grund Maxwellscher Vorstellungen *Arch. Elektrotech.* **2** 371–87

[7] Sillars R 1937 The properties of a dielectric containing semiconducting particles of various shapes *J. Inst. Electr. Eng.* **80** 378–94

[8] Bruggeman V D A G 1935 Berechnung verschidener physikalischer Konstanten von heterogenen Substanzen *Ann. Phys., Lpz.* **24** 636–79

[9] van Beek L K H 1960 The Maxwell–Wagner–Sillars effect describing apparent dielectric loss in inhomogeneous media *Physica* **26** 66–8

[10] Tinga W R, Voss W A G and Blossey D F 1973 Generalized approach to multiphase dielectric mixture theory *J. Appl. Phys.* **44** 3897–902

[11] Bergman D 1979 The dielectric constant of a simple cubic array of identical spheres *J. Phys. C: Solid State Phys.* **12** 4947–60

[12] Milton G W 1981 On the complex permittivity of a two-component composite material *J. Appl. Phys.* **52** 5286–93

[13] Clerc J P, Giraud G, Laugier J M and Luck J M 1990 The electrical conductivity of binary disordered systems, percolation clusters, fractals and related models *Adv. Phys.* **39** 191–308

[14] Sareni B, Krähenbühl L and Beroual A 1996 Complex effective permittivity of a lossy composite material *J. Appl. Phys.* **80** 4560–5

[15] Cummings K D, Garland J C and Tanner D B 1984 Optical properties of a small-particle composite *Phys. Rev.* B **30** 4170–82

[16] Tuncer E and Gubanski S M 1998 Dielectric properties of different composite structures *DRP'98: Dielectric and Related Phenomena* ed A Wlochowicz and E Targosz-Wrona (Bellingham, WA: SPIE Optical Engineering Press)

[17] Ferry D, Barker J R and Jacoboni C 1990 (ed) *Granular Nanoelectronics (NATO ASI Series B: Physics, vol 251)* (New York: Plenum)
[18] Lux F 1993 Models proposed to explain the electrical conductivity of mixtures made of conductive and insulating materials *J. Mater. Sci.* **28** 285–301
[19] Tsangaris G M, Kouloumbi N and Kyvelidis S 1996 Interfacial relaxation phenomena in particulate composite epoxy resin with copper or iron particles *Mater. Chem. Phys.* **44** 245–50
[20] Karasek L, Meissner B, Asai S and Sumita M 1996 Percolation concept: polymer-filler gel formation electrical conductivity and dynamic electric properties of carbon-black-filled rubbers *Polym. J.* **28** 121–6
[21] Wang S F and Ogale A A 1993 Continuum space simulations and experimental characterization of electrical percolation behavior of particulate composites *Composite Sci. Technol.* **46** 93–103
[22] Steeman P A M and Maurer F H J 1990 Dielectric monitoring of water absorption in glass-bead-filled high density polyethylene *Colloid Polym. Sci.* **286** 315–50
[23] Arous M, Kallel A, Fakhfakh Z and Perrier G 1997 Maxwell–Wagner–Sillars relaxations in surface-modified glass-bead polystyrene-based composites *Composite Interfaces* **5** 137–53
[24] Macdonald J R (ed) 1987 *Impedance Spectroscopy* (New York: Wiley)
[25] Gäfvert U and Nettelblad B 1990 Measurement techniques for dielectric response characterization at low frequencies *NORD-IS'90 Nordic Insulation Symp. (Lyngby)* pp 7:1–10
[26] Pollak M and Geballe T H 1961 Low frequency conductivity due to hopping processes in silicon *Phys. Rev.* **122** 1742–53
[27] Mott N F and Davis E A 1979 *Electronic Processes in Non-Crystalline Materials* (Oxford: Oxford University Press)
[28] Capaccioli S, Lucchesi L, Rolla P A and Ruggeri G 1998 Dielectric response analysis of a conducting polymer dominated by the hopping charge transport *J. Phys.: Condens. Matter* **10** 5595–617
[29] Hill R M and Dissado L A 1982 The temperature dependence of relaxation processes *J. Phys. C: Solid State Phys.* **15** 5171–93
[30] Dallamagne L 1993 Water absorption in silicone rubber and dielectric response measurements *Diploma Work* SECRC/KH/TR-93/030 (ABB Corporate Research)
[31] Tuncer E, Gubanski S M, Lambrecht J and Bärsch R 1998 Thermally stimulated depolarization currents of silicone rubbers immersed in water *ICSD'98: IEEE Int. Conf. on Conduction and Breakdown in Solid Dielectrics (Sweden ABB Support AB)* (New York: IEEE) pp 193–7
[32] Jeffrey H D 1997 *Nonparametric Smoothing and Lack-of-Fit Tests* (New York: Springer)
[33] Krauss T P, Shure L and Little J N 1994 *Signal Processing Toolbox User's Guide* (Natick, MA: The MathWorks, Incorporated) (reprinted edition)
[34] van Turnhout J 1972 Thermally stimulated discharge of polymer electrets *Central Laboratorium, Delft, The Netherlands, Technical Report Communication* No 471